Relationship of Electrical Properties and Partical Size of Piezoelectric Ceramics Fabricated by Digital Light Processing 3D Printing

Kai Liu
Wuhan University of Technology
Jiaming Hu
Wuhan University of Technology
Yusheng Shi
Huazhong University of Science and Technology
Chenyang Zhou
Wuhan University of Technology
Yunfei Sun
Wuhan University of Technology
Song Zhang
Wuhan University of Technology
Rong Tu
Wuhan University of Technology
Qingqing Zhang
Wuhan University of Technology
Yuzhen Zhang
Wuhan University of Technology
Changxia Yin
Wuhan University of Technology
Shangyu Huang
Wuhan University of Technology
Huajun Sun (✉ huajunsun2021@163.com)
Wuhan University of Technology https://orcid.org/0000-0002-2299-7484

Research Article

Keywords: 3D printing, Digital Light Processing, BaTiO3 piezoelectric ceramics, particle size, electrical properties

Posted Date: December 6th, 2021

DOI: https://doi.org/10.21203/rs.3.rs-1119291/v1

Relationship of Electrical Properties and Partical Size of Piezoelectric Ceramics Fabricated by Digital Light Processing 3D Printing

Kai Liu[a,b], Jiaming Hu[b], Yusheng Shi[c], Chenyang Zhou[b], Yunfei Sun[b], Song Zhang[e], Rong Tu[e], Qingqing Zhang[b], Yuzhen Zhang[b], Changxia Yin[d], Shangyu Huang[b], Huajun Sun[a,b,d,*]

[a] *State Key Laboratory of Silicate Materials for Architectures, Wuhan University of Technology, Wuhan, 430070, Hubei, China*

[b] *School of Materials Science and Engineering, Wuhan University of Technology, Wuhan, 430070, Hubei, China*

[c] *State Key Laboratory of Materials Processing and Die & Mould Technology, Huazhong University of Science and Technology, Wuhan, 430074, Hubei, China*

[d] *Advanced Ceramics Institute of Zibo New & High-Tech Industrial Development Zone, Zibo, 255000, Shandong, China*

[e] *State Key Laboratory of Advanced Technology for Materials Synthesis and Processing, Wuhan University of Technology, Wuhan 430070, China*

*Corresponding author. Tel.: + 86 18553328129.

E-mail address: huajunsun@whut.edu.cn (H. Sun).

Abstract

To improve electrical properties of $BaTiO_3$ piezoelectric ceramics fabricated by 3D printing, effects of particle sizes was investigated on rheological and curing properties of ceramic slurries, electrical properties of $BaTiO_3$ fabricated by Digital Light Processing 3D printing method. It was found that the curing ability of ceramic slurries decreased first and then increased with the increase of particle size from 136 nm to 1486 nm, while the viscosity of the slurries kept decreasing. When the particle size in a range of submicron, the grain size of sintered ceramics decreased from 13.27 μm to 6.84 μm as particle size increasing. Immediately, the relative density, piezoelectric constant, relative permittivity and remanent polarization of sintered ceramics were measured and it turns out to reach 95.32%, 161.4 pC/N, 1512 and 7.59 uC/cm^2 respectively while using the $BaTiO_3$ powder with particle sizes of 993 nm. Finally, a cellular structural $BaTiO_3$ ceramics was fabricated by using optimized powder and process parameters and packaged as a piezoelectric sensor, showing a good function of force-electricity conversion. These results demonstrated the feasibility of fabricating high-quality functional ceramics with designed geometry by Digital Light Processing.

Keywords: 3D printing; Digital Light Processing; $BaTiO_3$ piezoelectric ceramics; particle size; electrical properties.

1 Introduction

Piezoelectric ceramics could realize the mutual conversion of mechanical and electrical energy relying on piezoelectric effect and were widely used in medical health, aerospace, underwater acoustic engineering and other fields [1]. Compared with lead containing piezoelectric ceramics, Lead-free $BaTiO_3$ ceramics have great potential for its low-cost and environmentally friendly advantages [2]. In order to meet the development needs of various complex and extreme environments, the requirements for the shape and structure of piezoelectric ceramics are increasing [3]. Nevertheless, it is much difficult to fabricate $BaTiO_3$ ceramics with complex shape by

conventional methods due to the dependence on the mold, such as dry pressing, injection molding, roll forming, and tape casting and etc [4-6].

Digital Light Processing (DLP), as one kind of 3D printing methods, is thought to be an effective way to fabricate complex-shape ceramic components using a “layer by layer” method. In recent years, 3D printing process has been used to form a variety of ceramics, such as alumina [7-9], zirconia [10], mullite [11], PZT [12] and $BaTiO_3$ [13-15]. Chen et al. [13] used DLP process to fabricate an ultrasonic transducer to realize the energy focusing and ultrasonic sensing. Zeng et al. [14] used this technology to prepare $BaTiO_3$-based piezoelectric composite ceramics with honeycomb-structure. Cheng et al. [15] fabricated $BaTiO_3$ ceramics with a piezoelectric constant (d_{33}) of 166 pC/N at 80% BTO weight percentage via DLP process. Although DLP process were widely used to fabricate piezoelectric ceramics with complex shape or internal structure, the density and properties of the piezoelectric ceramics formed by this method were relatively lower than those using traditional methods [16]. Particle sizes might have influences on the density and properties of piezoelectric ceramics according to the research on piezoelectric ceramics prepared by traditional methods. Liu et al. [17] fabricated PbO based piezoelectric ceramics precursor powder with different particle mean sizes by using high-energy vibration ball milling and planetary ball milling, and found that the powder with coarser particle sizes had a larger piezoelectric constant (d_{33} = 87 pC/N) when sintered at 1180°C. Huan et al. [18] fabricated $BaTiO_3$ disks in dry pressing to analyze the grain size influence on the piezoelectric property by evaluating different settings for a two-step sintering process, achieving a grain size of 1 um and a maximum d_{33} of 519 pC/N. However, there are currently few studies on improving the properties of 3D printed piezoelectric ceramics.

This paper describes a DLP process to fabricate high-performance $BaTiO_3$ piezoelectric ceramics through the investigate of particle size effect. The effects of different particle sizes on the rheological behavior and curing properties of the slurries were discussed. Furthermore, the microstructure and electrical properties of sintered bodies with different particle sizes were characterized. Finally, a cellular structural

$BaTiO_3$ ceramics was obtained by using optimized powder and process parameters via DLP, and its composites were fabricated and made into piezoelectric sensor to verify force-electricity conversion function.

2. Experimental details

2.1 Materials and Preparation of ceramic slurry

Five kinds of $BaTiO_3$ powder (Hongde Nanomaterials, Nanjing, China) were used to evaluate the effect of particle size，with d_{50} of 136, 197, 355，993 and 1486 nm respectively. The particle size distribution is shown in Fig. 1. Triton X-100 (Phygene Life Sciences, Fuzhou, China) was used as surfactant. MPDISP (MeiPai Industrial, Shanghai, China) were used as dispersant to prevent ceramic particles from gathering and settling. Acryloylmorpholine (ACMO, Japan KJ Chemicals) was used as the photosensitive monomer to bind $BaTiO_3$ powder for ceramic slurry. TPO (IGM Resins, Netherlands) and 4-Methoxyphenol (MEHQ, Sinopharm Chemical Reagent, China) were used as the photoinitiator and polymerization inhibitor respectively. Cellular ceramic was filled with E51 epoxy resin(Suixin Chemical, Guangzhou, China) and packaged with polydimethylsiloxane (PDMS, Dow Corning, America) to obtain a piezoelectric sensor.

ACMO monomer was firstly mixed with TPO and MEHQ to obtain a photosensitive resin, and then it was put into a planetary ball mill together with ceramic particles, which was employed at 200 r/min for 4 h. Finally, the $BaTiO_3$ slurry was vacuum defoamed for 20 min in a vacuum drying oven at a room temperature.

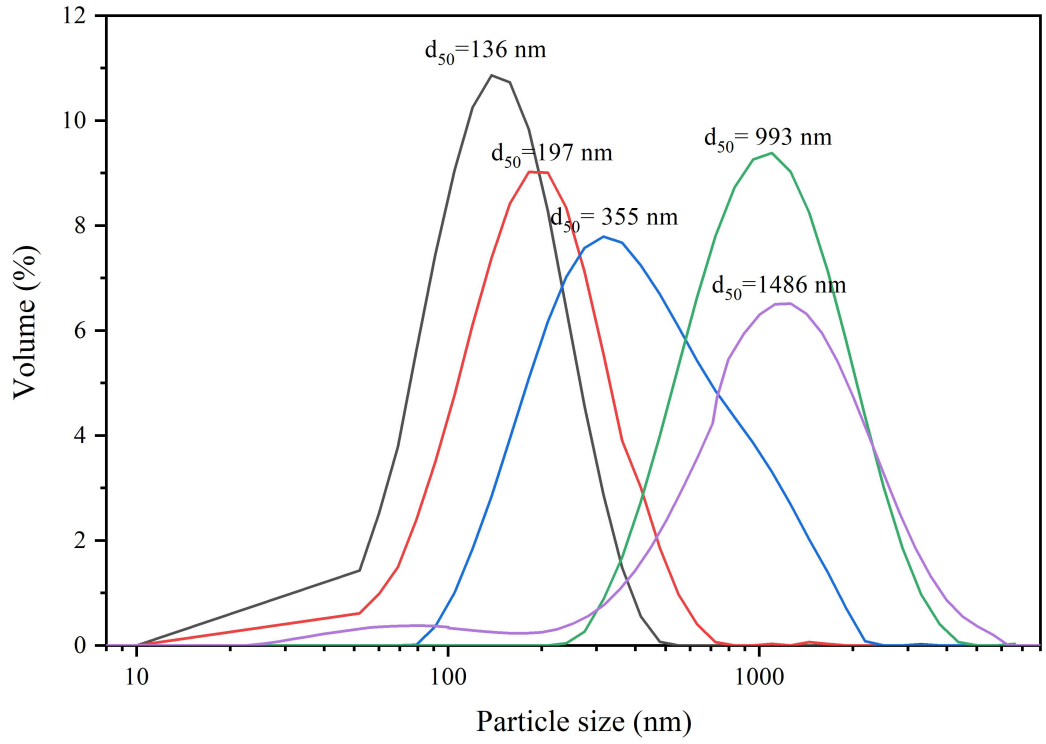

Fig. 1 $BaTiO_3$ particle size distribution.

2.2 DLP process

Under the irradiation of ultraviolet light, the monomers are cross-linked to form a dense three-dimensional network structure, and the ceramic powder is fixed in it to form a stable three-dimensional structure. Different from the curing characteristics of pure photosensitive resin, the light will be scattered by the ceramic particles in the highly concentrated $BaTiO_3$ slurry. The curing properties of ceramic slurry can be evaluated by curing depth (C_d), which can be described with the Eq. (1) [19]:

$$C_d = \frac{2d_{50}}{3\tilde{Q}} \frac{n_0^2}{\Delta n^2} \ln\left(\frac{E_0}{E_c}\right) \quad (1)$$

where d_{50} is the particle mean size of ceramic particles, $\tilde{Q}$ is the scattering efficiency term, Δn^2 is the square of the difference between the ceramic refractive index (n_p) and medium refractive index (n_0), E is the energy density, and E_C is the critical energy density. The scattering efficiency $\tilde{Q}$ is related to particle spacing S and ultraviolet (UV) wavelength λ, and can be described with the Eq. (2) [19].

$$\tilde{Q} \propto \frac{S}{\lambda} \tag{2}$$

Fig. 2 describes a schematic diagram of the DLP printer. The printing platform moves below the liquid level of the slurry tank, and the sliced graphics can be projected onto the bottom of the resin tank. The height of the printing platform is controlled so that a liquid thin layer can be formed between the printing platform and the release film. When the ultraviolet light is turned on, the liquid thin layer will be formed to a cured layer of a specific shape attached to the printing platform according to the projection pattern. Then the UV light is turned off, the printing platform moves upward to separate the cured layer from the release film. Meanwhile, the doctor blade scrapes the remaining slurry, and a thin liquid layer is formed between the release film and the cured layer. Then the second layer of slurry is cured, and is bonded to the first cured layer through photopolymerization reaction. And so on, the green body will be manufactured layer by layer.

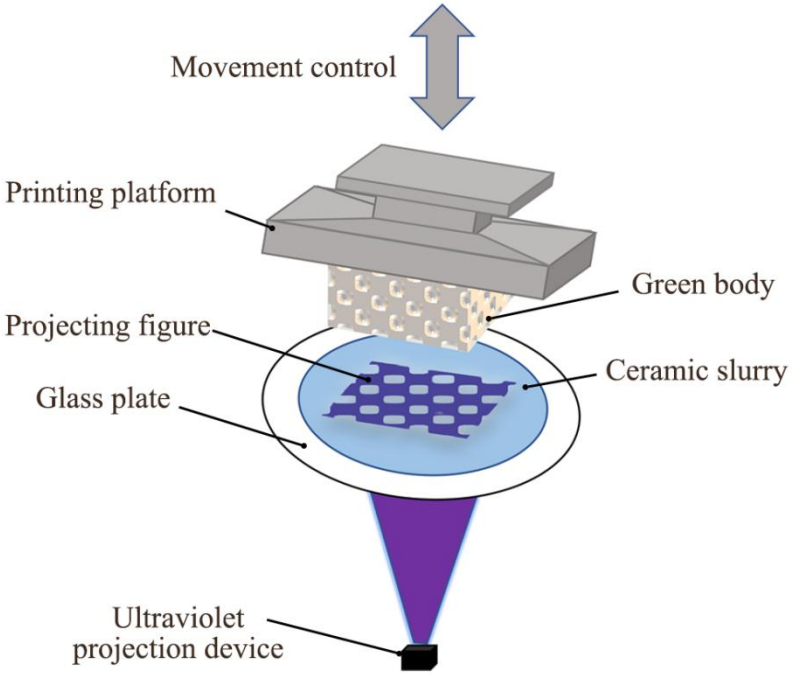

Fig. 2 Structure of the DLP printing machine.

2.3 Post-processing

The green body formed by DLP process contains about 20 wt% of resin and additives, which likely lead to defects such as cracks and delamination during the debinding and sintering process. To obtain piezoelectric ceramics with excellent properties, a reasonable heat treatment process must be developed to remove the internal organic components and densify the ceramic. The main factors affecting debinding process include atmosphere, heating rate, holding time and holding node. Nitrogen-air debinding system was used in this study to delay the decomposition of organic matter.

The TG-DSC test results of the green body in a nitrogen atmosphere is shown in Fig. 3. A weight reduction of 1% before 230°C due to the evaporation of water, and then the weight has a heavy drop with the increaseing temperature. The stage with the greatest weight loss is observed between 350°C and 550°C due to the removal of resin. An obvious peak appears at 421.8°C caused by the decomposition of the resin accompanied an exothermic reaction. Therefore, the debinding process in a nitrogen atmosphere was set to a slow heating rate of 0.5°C/min, which could release the generated gas and reduce internal stresses. During the heating period, the temperature was kept at 300, 400, 450, 500, 600 and 700°C for 1 hour respectively, so that the organic matter could be fully converted into carbon. Then the carbonized body was heated to 800°C at 1°C/min under air atmosphere, and kept at 450, 600 and 800°C for 2h respectively to remove carbon. Finally, the temperature was raised to 1210°C-1330°C at 3°C/min and sintered for 2 hours. The debinding and sintering curve are shown in Fig. 4.

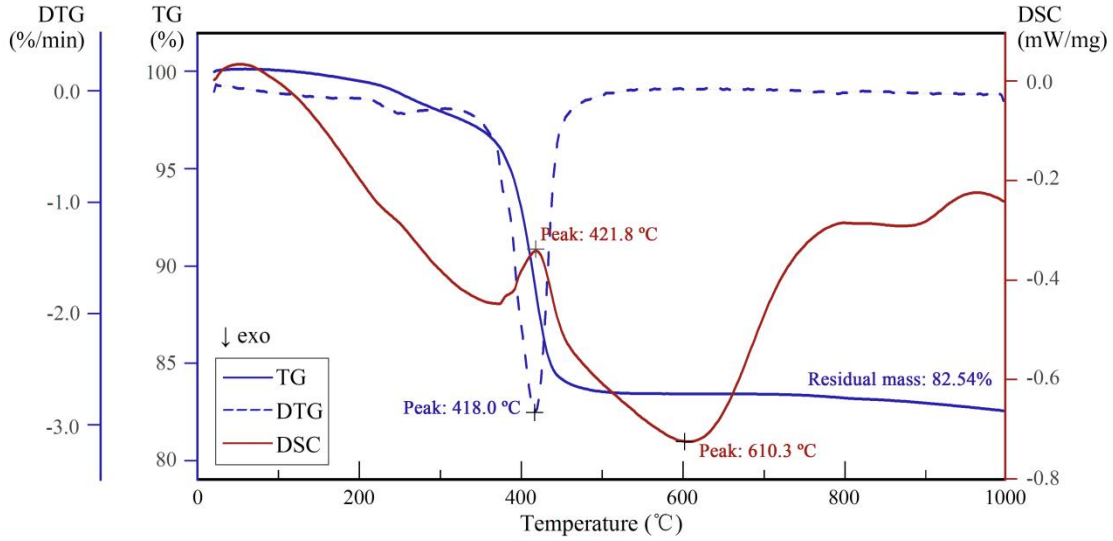

Fig. 3 TG-DSC test results of the green body in a nitrogen atmosphere.

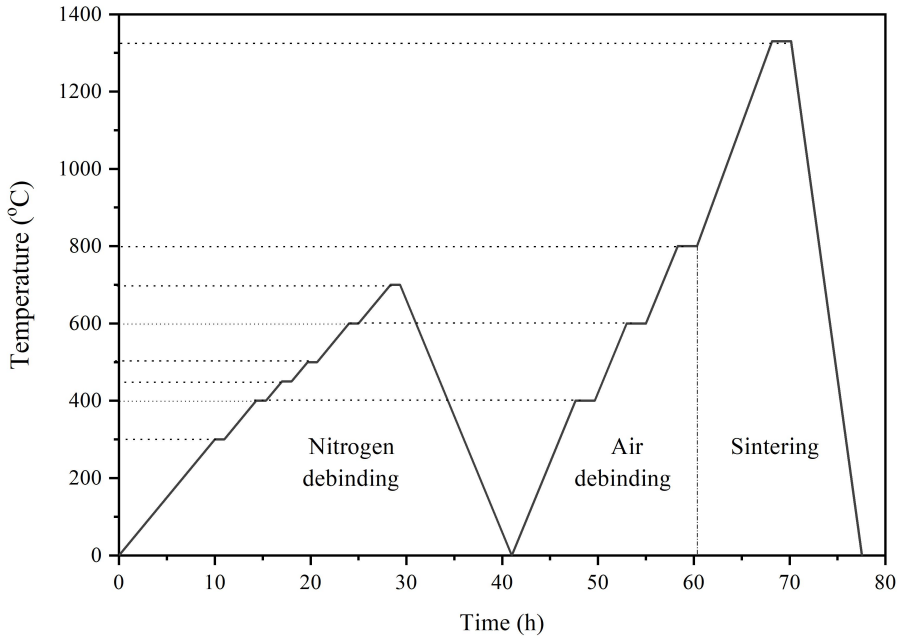

Fig. 4 Nitrogen-air debinding and sintering process.

Fig. 5 shows the surface and side morphology changes of the bodies at various stages. During debinding and sintering process, the green body gradually denser. After sintering, both the top and bottom surfaces of the ceramics were coated with silver ink as the electrodes, and then polarized in an silicon oil bath at 60°C for 15 min under an electric field of 2 kV/mm. The piezoelectric composites in this paper are prepared by impregnating ceramic samples with epoxy resin and curing agent at a mass ratio of 3:1, and any excess epoxy beyond the surfaces was removed with a cutter.

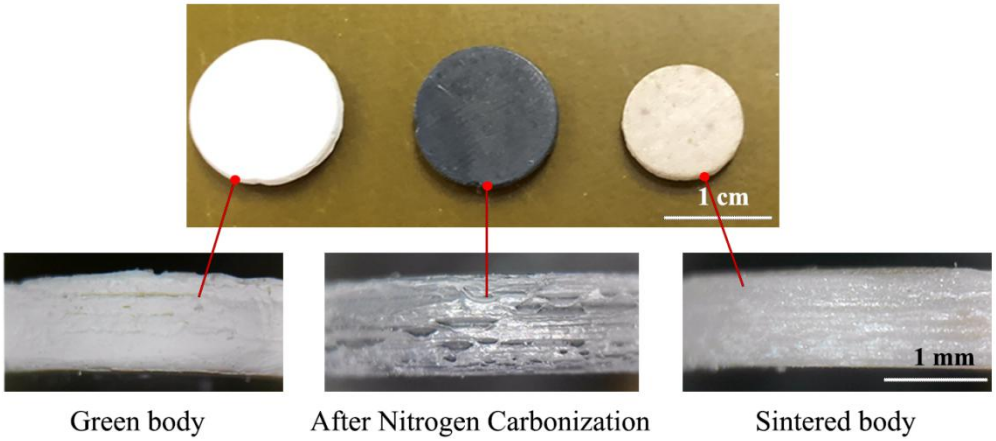

Fig. 5 The surface and side of bodies of each stage.

2.4 Characterization and testing

The ceramic green body was prepared by ceramic DLP 3D printer (Ceraform 100, Shenzhen Changlang Technology Co. China) with an UV source of λ = 405 nm and a light intensity of 8 mW/cm^2. The particle size distribution of the ceramic particles was tested by a laser particle size analyzer (Mastersizer 2000, Malvern Panalytical, UK). The rheological properties of the slurry were tested by a rotary rheometer (RheolabQC, AntonPaar, Austria). The microstructures of samples were observed by a scanning electron microscopy (SU8010, Hitachi, Japan). The TG-DSC analysis was performed by a simultaneous thermal analyzer (TGA/DSC 3+, METTLER TOLEDO, USA). The density of the sintered samples was measured by the Archimedes method. The phase analysis was carried out by an X-ray diffractometer (D8 Advance, Bruker, Germany). The dielectric properties was measured by an impedance analyzer (1260A+1296A, Solartron Analytical, UK). The piezoelectric constant was tested by a quasi-static d_{33} meter (ZJ-4AN, Institute of Acoustics, Chinese Academy of Sciences). The ferroelectric properties was measured by a ferroelectric analyzer (RTI-Multiferroic, Radiant, USA).

3. Results and discussion

3.1 Rheological behavior of slurries

Five particle sizes of $BaTiO_3$ powder were used to formulate 80 wt% ceramic

slurry. The changes in viscosity and shear stress with shear rate are shown in Fig. 6. It can be seen that all groups of slurries were shearing thinning at high shear rates, indicating that the ceramic particles were better dispersed in the resin. The initial viscosity of slurry with finer particles was higher at low shear rate, and the viscosity gap was gradually narrowed with the increaseing shear rate. Generally, as the particle size of the ceramic powder decreases, the viscosity and shear stress of slurry will increase. Finer particles are more affected by the van der Waals force [20], resulting in agglomeration of particles in the slurry, which increases the contact between the particles. The fluid will be trapped in the powder aggregates, thereby increasing the viscosity of the suspension. Excessive viscosity will affect the self-leveling of the slurry during the printing process. Therefore, powder with coarser particle size is easier to disperse in the slurry and more likely to be printed in terms of the rheological properties of the slurry.

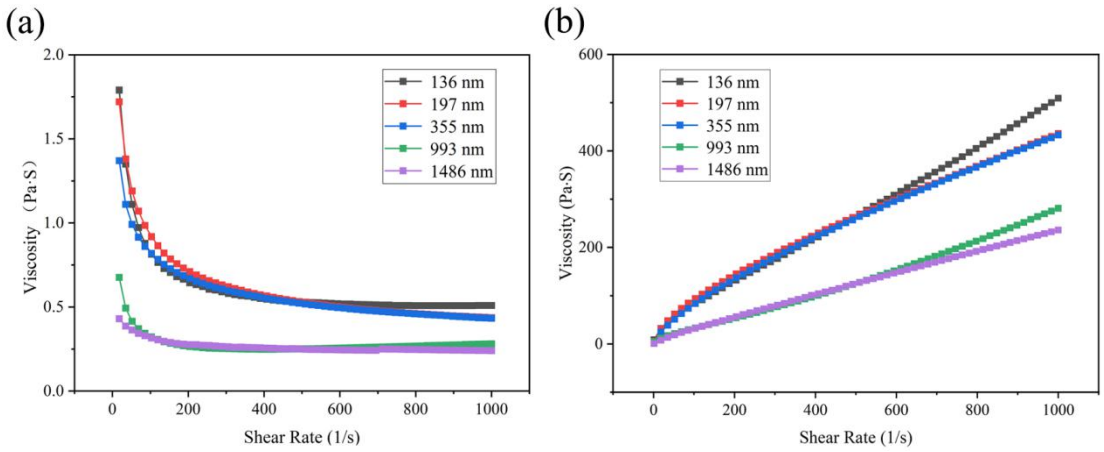

Fig. 6 Rheological properties of slurries with different particle mean size. (a) Viscosity changes with shear rate; (b) Shear stress changes with shear rate.

3.2 Curing properties of slurries

Within a certain exposure time, the slurry forms a solidified layer of a certain thickness in the direction perpendicular to the projection surface. This thickness is called the curing depth, which can be used to evaluate the curing ability of the slurry. On the one hand, too short exposure time will lead the low curing depth, resulting in poor bonding between the layers of the blank and easy to fall off during printing. On the other hand, too long exposure time will increase the overcure ratio and affect

printing accuracy. Therefore, the printing parameters need to be strictly controlled according to the curing properties of different slurries. Fig. 7 shows the relationship between the cured depth and the particle size under different exposure times. It can be seen that with the increase of powder particle size, the curing depth showed a trend of decreasing first and then increasing. Moreover, extending the exposure time can significantly increase the curing depth.

According to Eq. (1), the curing ability of slurry is related to particle size and scattering efficiency under the condition of certain material and light intensity. In this study, the wavelength of ultraviolet light emitted by the printer is 405 nm. It was mentioned in the previous section that the finer particles were more likely to producing agglomerations in the slurries, resulting in the reduction of the particle spacing. With $\widetilde{Q} \propto S / \lambda$ and λ = 405 nm, $\widetilde{Q} < 1$ for the fine powder, and $\widetilde{Q} > 1$ for the coarse powder. When the particle size is small, the agglomeration of particles is obvious, and the S is much smaller than the λ. At this time, the scattering efficiency of the slurry is the dominant factor, so that the curing depth decreases gradually with the increaseing particle size. As the particle size increases, the particles are uniformly dispersed in the slurry, and the S is greater than the λ. At this time, the particle characteristics in the slurry are the dominant factor, so that the curing depth increases gradually. This is consistent with previous reports [19,21]. Then, the optimal printing parameters were selected based on the curing ability of the slurrries, as shown in Table 1.

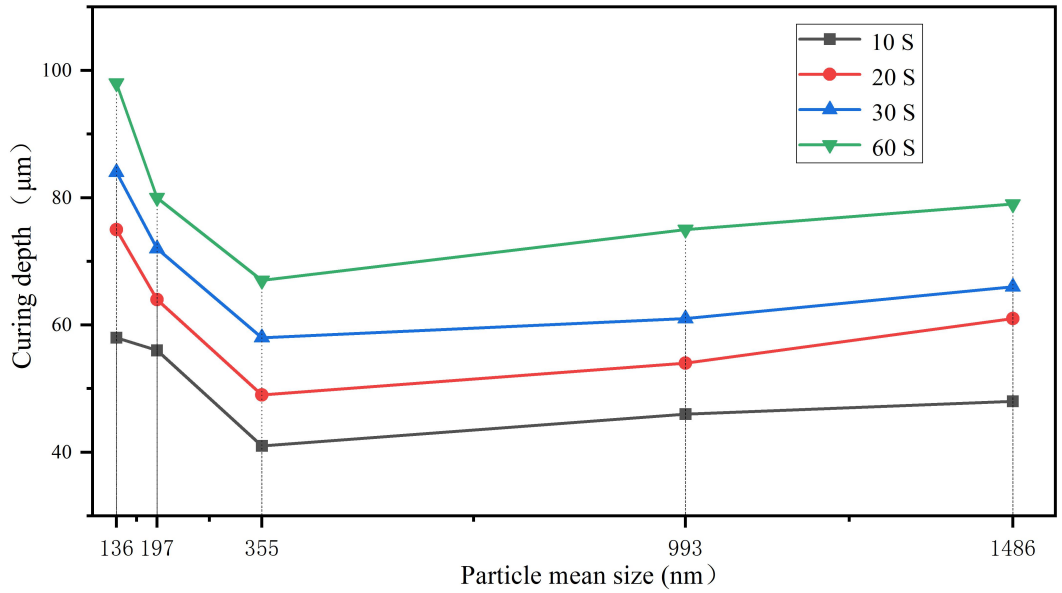

Fig. 7 Curing properties of slurries with different particle size.

Table 1 Parameters about preparing of $BaTiO_3$ ceramics by DLP

d_{50} (nm)	136	197	355	993	1486
layer thickness (μm)	30	30	30	30	30
Main layers exposure time (s)	10	12	30	20	15

3.3 Sintering parameter

The relationship between the density and sintering temperature is shown in Fig. 8. With the increase of the sintering temperature, the density of the 136 nm and 197 nm samples significantly decreases, the maximum of which were 5.31 g/cm^3 and 5.27 g/cm^3 respectively (relative density were 88.20% and 87.54% respectively). While the density of the 355 nm and 997 nm samples reached a maximum density of 5.49 g/cm^3 (relative density was 91.23%) at 1250°C and 5.74 g/cm^3 (relative density is 95.32%) at 1330°C respectively. When the particle size is in the submicron range, coarser particles need to be sintered at higher temperatures to obtain relatively dense ceramics. Due to the higher specific surface energy of fine particles, less energy is required in the sintering process. As the particle size increases to 1486 nm, the density of the sintered sample is lower than that of 993 nm sample at all temperatures in the test range. This can be interpreted that the coarser powder reduce the contact area and

increase the pores between the particles, while the volume of grain growth cannot fill this part completely.

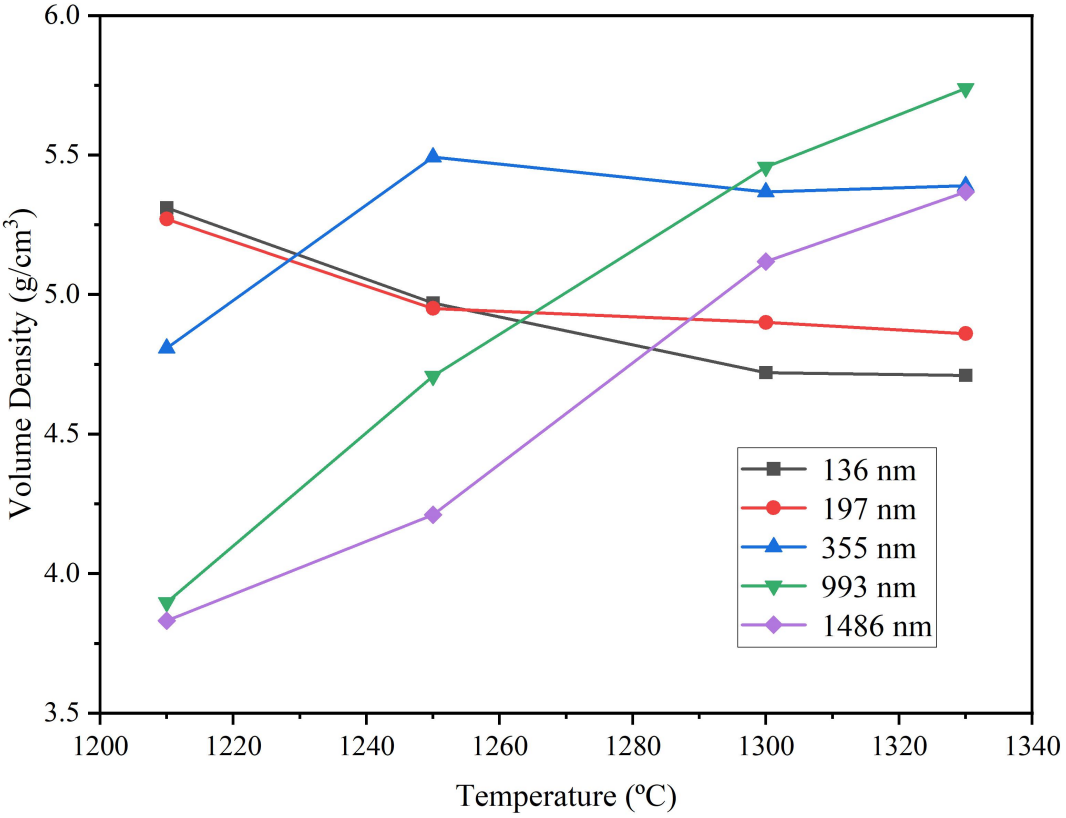

Fig.8 Density of Sintered bodies with temperature.

3.4 Micro morphology and XRD analysis

Fig. 9(a) shows the samples sintered at 1330°C with a particle size of 136 nm. The average grain grow of about 13.27 μm was observed, and there were many pores between the grains. The 197 nm, 355 nm and 993 nm samples are illustrated in Fig. 9(b), (c) and (d) respectively. In the submicron range， the average grain size of sintered samples gradually decreased to 11.56 μm, 9.23 μm and 6.84 μm with the increasing particle size. Meanwhile, a reduction on the number of pores and pores sizes were observed. Studies have shown that the final grain size after sintering is highly related to the sintering temperature, sintering time and powder particle size [22,23]. Ceramic powder with a finer particle size has a higher curvature. Therefore, the grain growth is larger under the same sintering temperature and time. While as the particle size increases to the micron range (Fig. 9(e)), it is susceptible to the influence of small impurity particles, which hinders the normal growth of crystal grains and

leads to secondary crystallization.

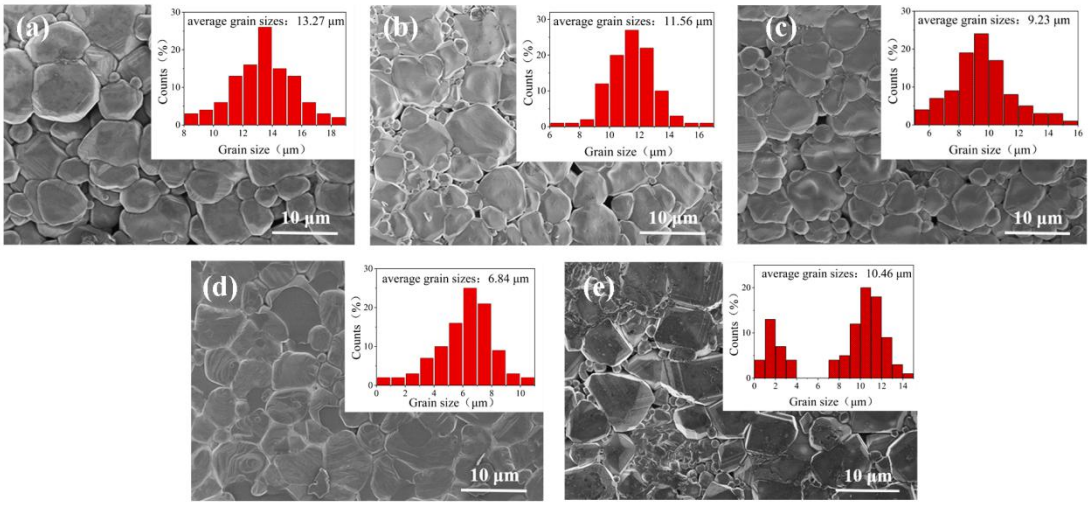

Fig. 9 Cross-sectional SEM micrographs of $BaTiO_3$ sintered 1330°C with different particle mean size. (a) 136 nm; (b) 197 nm; (c) 355 nm; (d) 993 nm; (e) 1486 nm.

The XRD patterns of Sintered $BaTiO_3$ are shown in Fig. 10. The samples were evaluated at room temperature. The peaks observed index for tetragonal crystal structure [24]. In addition, the peaks splitting observed around at 45°, 51° and 56° indicates a phase transformation from cubic structure. Moreover, The 993 nm sample shows a weak peak splitting intensity, which indicates a decrease in the content of the tetragonal phase. The tetragonal property decreases due to the increase of strain caused by the high surface area of fine grains.

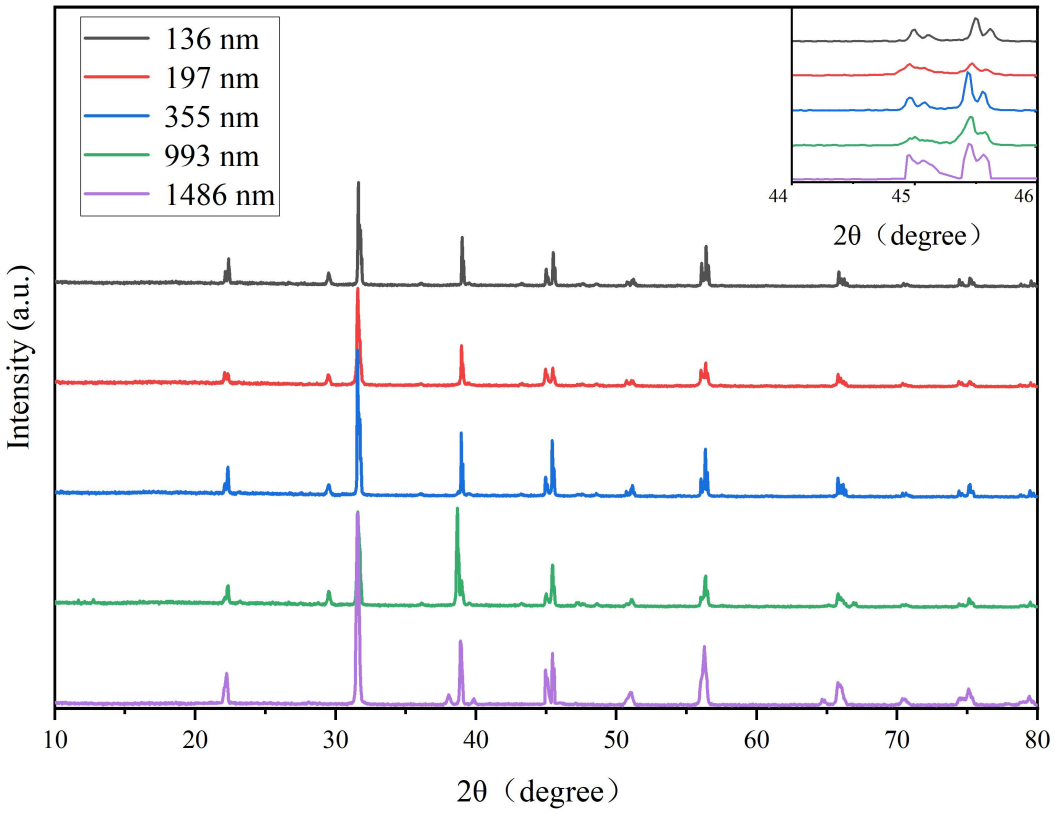

Fig. 10 XRD patterns of Sintered samples with different particle mean size.

3.5 Material properties

Fig. 11 indicates the relationship between the piezoelectric constant and relative permittivity (ε_r) of the samples sintered at 1330°C and the particle sizes. The d_{33} were 108.2 ± 7.2 pC/N, 121.3 ± 8.8 pC/N, 134.1 ± 9.3 pC/N, 161.4 ± 7.2 pC/N and 122.4 ± 7.6 pC/N for the 136 nm, 197 nm, 355 nm, 993 nm and 1486 nm respectively. And the relative permittivity at 1 kHz were 718 ± 28, 760 ± 32, 948 ± 51, 1512 ± 62 and 734 ± 30 respectively. The properties of the sintered samples are closely related to the density and porosity. A depolarization field will be generated on the surface of the pores, which will affect the movement of the domain wall during the polarization process. It can be seen from Fig. 8 and Fig. 9 that with the increase of particle size, the density of the samples increase and the pores gradually decrease when sintered at 1330°C. But as the particles grow to 1486 nm, Large particles with irregular shape are accompanied by an increase in porosity. Therefore, the 993 nm sintered samples showed better piezoelectric and dielectric properties. In addition, the crystal grain size

will also affect the piezoelectric and dielectric properties. The grain size of sintered samples decreased from 13.27 μm to 6.84 μm. Since the average width of the domain decreases with the decrease of the crystal grain size, which means that the density of the domain wall increases with decreasing grain size. This might contribute to a maximum in domain wall activity, resulting in a maximum in piezoelectric properties and dielectric properties of the samples. This is also as previously reported [25,26].

Fig. 12 shows the polarization-electric field (*P-E*) hysteresis loop of the samples under the maximum electric field of 30 kV/cm, and the frequency was 20 Hz. It can be seen that all of the ceramics show slim P-E hysteresis loops. In addition, the remnant polarization (P_r) of the samples change from 20.25 uC/cm^2 to 7.59 uC/cm^2 . It is mainly attributed to the grain size effect of ceramics. Due to the high proportion of the surface of fine-grained, the crystal field generated in the crystal grains is weak, resulting in poor long-range interaction between dipoles as well as poor ferroelectricity.

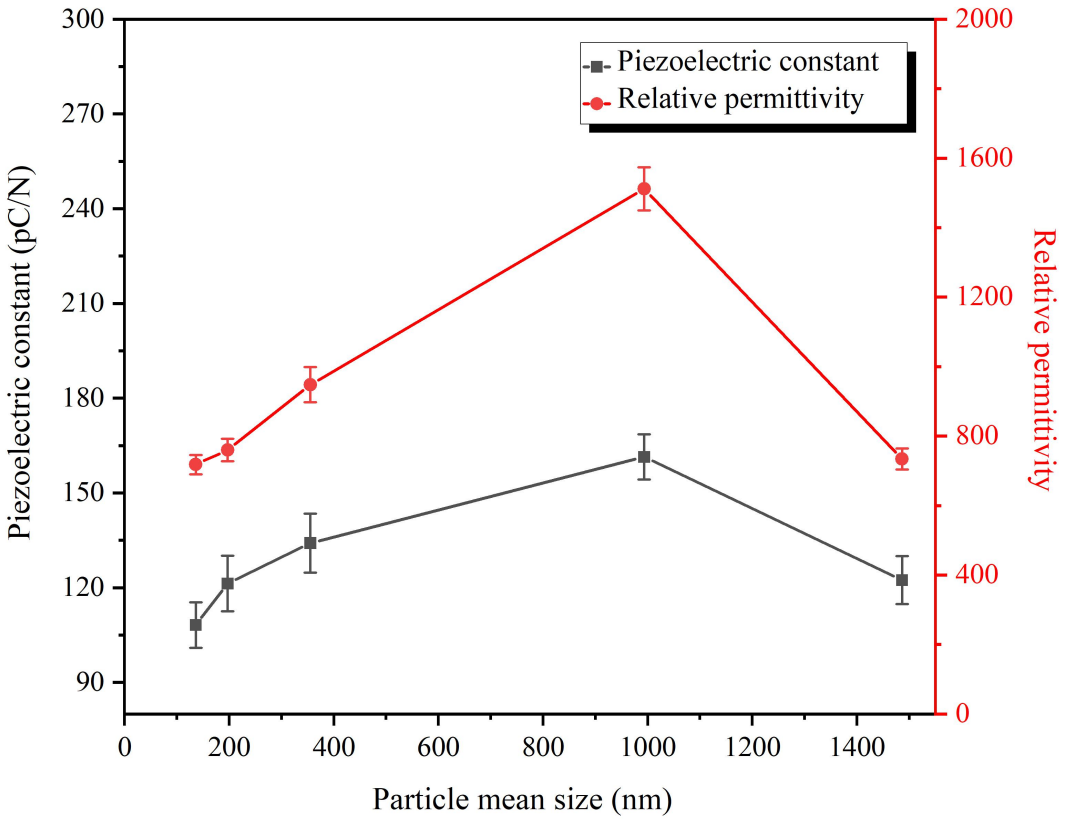

Fig. 11 Piezoelectric constant and relative permittivity properties of sintered body with different particle mean size.

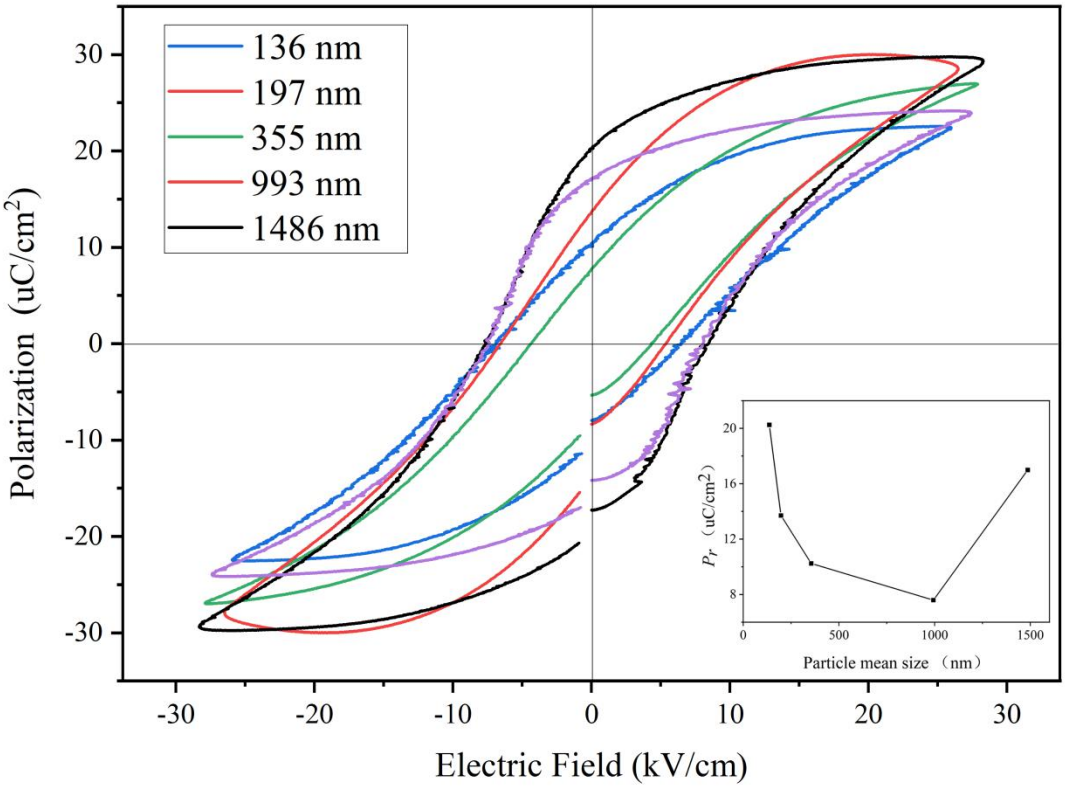

Fig. 12 Ferroelectric properties of sintered body with different particle mean size.

3.6 Piezoelectric sensor

To verify the feasibility of DLP process in forming complex structures and evaluate the properties of the printed $BaTiO_3$ ceramics, a face-centered cubic (FCC) structure $BaTiO_3$ ceramics (Fig. 13(a) and (b)) was designed and fabricated by using optimized powder and process parameters based on the DLP process, and epoxy resin was filled inside (Fig. 13(c)). The interfaces of the FCC structure provide significantly higher stress transfer efficiency, which subsequently contributes to the excellent electrical properties with a d_{33} of 112 pC/N. Electrodes and wires were adhered to the surfaces of the piezoelectric composites, and then the entire sample was encapsulated by a flexible polymer (polydimethylsiloxane, PDMS) to obtain a piezoelectric sensor (Fig. 13(d)).

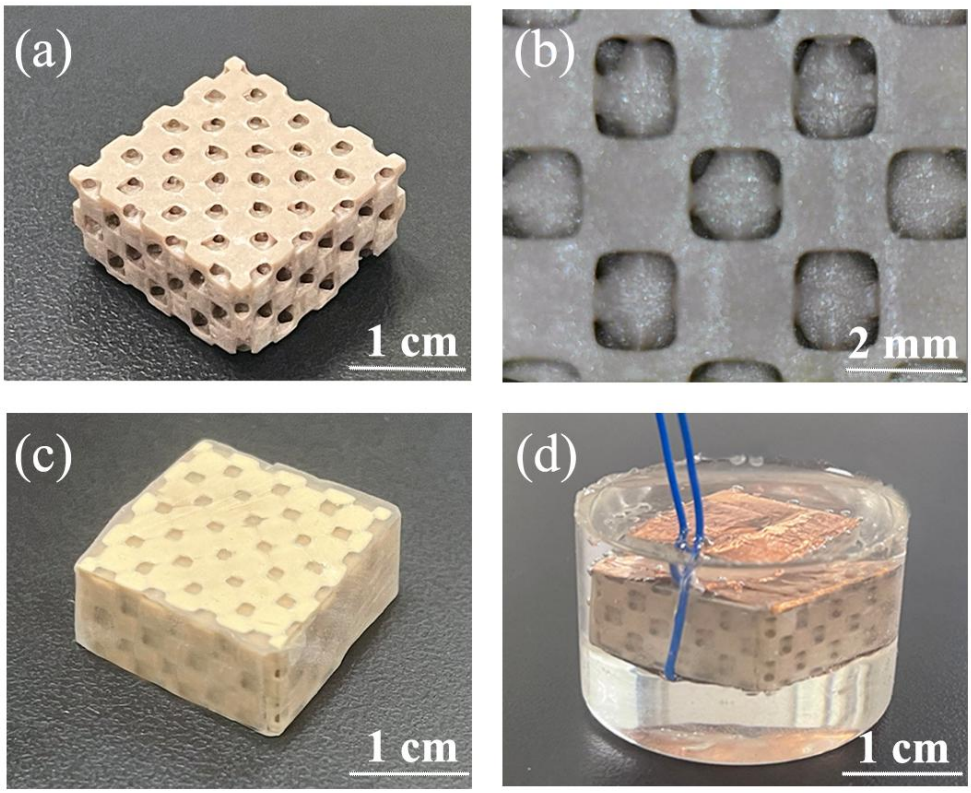

Fig.13 Complex-structured $BaTiO_3$ ceramics and composites fabricated by DLP process. (a) sintered ceramics; (b) Surface magnified photo of sintered ceramics; (c) $BaTiO_3$/Epoxy piezoelectric composites; (d) Piezoelectric sensor.

Fig. 14 shows a proof-of-concept experimental system, which mainly includes a force applying device, a voltage testing meter and the piezoelectric sensor. The force applying device on the right can perform a cyclic movement with a certain displacement amplitude, providing a cyclic force for the piezoelectric sensor. When the device on the right moves, the piezoelectric sensor is stressed and an electrical signal is generated. Then the electrical signal propagates through the wire to the voltage testing meter, forming a series of waveforms. When the displacement amplitude changes from 1 mm to 5 mm, the stress on the piezoelectric sensor will increase, and the amplitude of the voltage increase from 0.25 V to 1.5 V, as shown in Fig. 15.

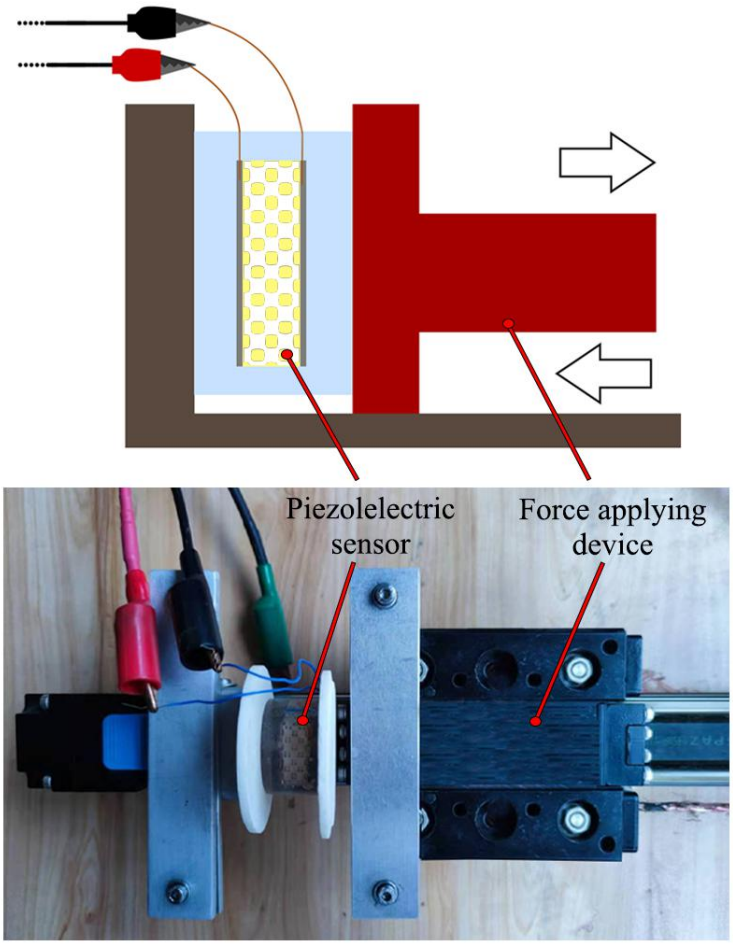

Fig.14 Testing procedures for voltage responses of piezoelectric sensor.

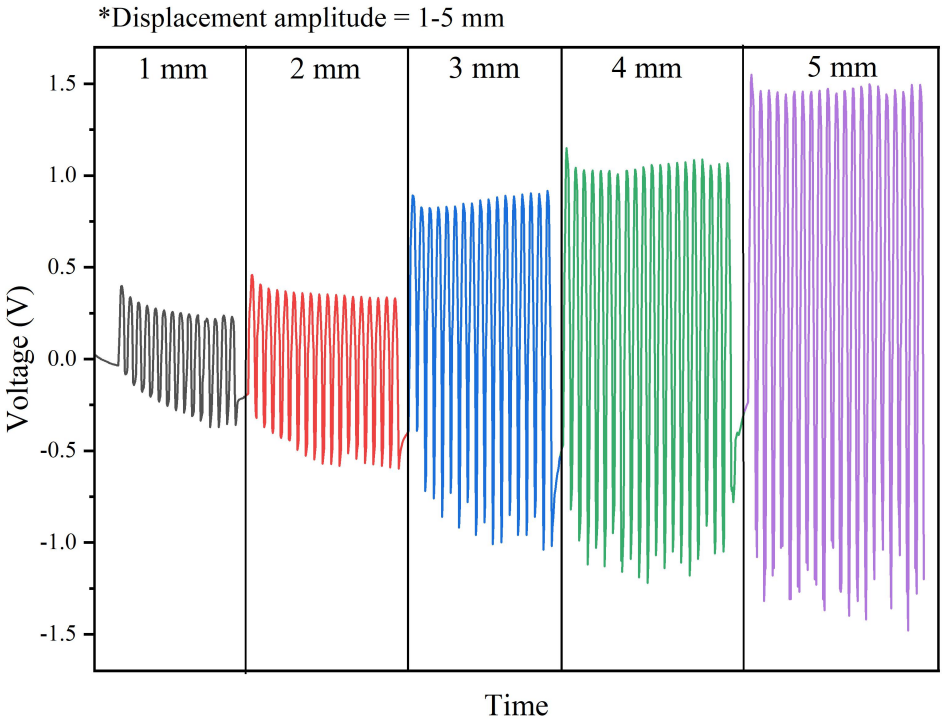

Fig.15. The output voltage changes with the displacement amplitude.

4 Conclusions

Relationship of electrical properties and partical size on dielectric, piezoelectric and ferroelectric properties of $BaTiO_3$ fabricated by DLP were studied. The results show that the $BaTiO_3$ powder with 993 nm particle mean size grains grew of 6.84 μm, and the best piezoelectric and dielectric properties was obtained, reaching 161.4 pC/N and 1512 respectively. While the ferroelectric properties had the lowest performance. This is determined by the grain size obtained by sintering. Moreover, different particle sizes of $BaTiO_3$ were investigated in terms of the effects on the rheological and curing properties for the slurries. The curing ability of slurry was weak when the particle size is close to the ultraviolet wavelength. Finally, The force-electricity conversion functional were initially realized in the self-built experimental scene, which laid the foundation for the further manufacture of complex-structured piezoelectric materials with shock absorption and self-monitoring functions.

Acknowledgments

This work was supported by the National Key Research and Development Plan，Hubei High Value Patent Cultivation Project（2021pm0012），the National Natural Science Foundation of China （U1806221, 51672198）, Innovation and Development Project of Zibo City （2017CX01A022）, Instruction & Development Project for National Funding Innovation Demonstration Zone of Shandong Province（2017-41-1, 2017-41-3, 2018ZCQZB01, 2019ZCQZB03）, Central Guiding Local Science and Technology Development Special Funds （2060503） and Key Research & Design Program of Shandong Province （2019GGX102011）.

References

[1] Elahi H, Munir K, Eugeni M, et al. A Review on Applications of Piezoelectric Materials in Aerospace Industry. Integrated Ferroelectrics 2020, **211**: 25-44.

[2] Shrout TR and Zhang SJ. Lead-free piezoelectric ceramics: Alternatives for PZT? Journal of Electroceramics 2007, **19**: 113-126.

[3] Lu ZL, Cao JW, Song ZQ, et al. Research progress of ceramic matrix composite parts based on additive manufacturing technology. Virtual and Physical Prototyping 2019, **14**: 333-348.

[4] Asif A, Nazir R, Riaz T, et al. Influence of processing parameters and solid concentration on microstructural properties of gel-casted porous hydroxyapatite. Porous Mater 2014, **21**: 31-37.

[5] Moreno R, Salomoni A, Stamenkovic I, et al. Colloidal filtration of silicon nitride aqueousslips, part two: slip casting and pressure casting performance. Journal of the European Ceramic Society 1999, **19**: 49-59.

[6] Prabhakaran K, Kumbhar CS, Raghunath S, et al. Effect of concentration of ammonium poly(acrylate) dispersant and MgO on coagulation characteristics of aqueous alumina direct coagulation casting slurries. Journal of the American Ceramic Society 2008, **91**: 1933-1938.

[7] Shuai X, Zeng Y, Li P, et al. Fabrication of fine and complex lattice structure Al_2O_3 ceramic by digital light processing 3D printing technology. Journal of Materials Science 2020, **55**: 6771-6782.

[8] Liu SS, Li M, Wu JM, et al. Preparation of high-porosity Al_2O_3 ceramic foams via selective laser sintering of Al_2O_3 poly-hollow microspheres. Ceramics International 2020, **46**: 4240-4247.

[9] Dong Y, Jiang HY, Chen AN, Yang T, et al. Near-zero-shrinkage Al_2O_3 ceramic foams with coral-like and hollow-sphere structures via selective laser sintering and reaction bonding. Journal of the European Ceramic Society 2021, **41**: 239-246.

[10] Chen F, Zhu H, Wu JM, et al. Preparation and biological evaluation of ZrO_2 all-ceramic teeth by DLP technology. Ceramics International, 2020, **46**: 11268-11274.

[11] Chen AN, Meng L, Wu JM, et al. Enhancement mechanism of mechanical performance of highly porous mullite ceramics with bimodal pore structures prepared by selective laser sintering. Journal of Alloys and Compounds 2019, 776:486-494.

[12] Chen Y, Bao X L, Chi-Man Wong, et al. PZT ceramics fabricated based on stereolithography for an ultrasound transducer array application. Ceramics International 2018, **44**: 22725-22730.

[13] Chen Z, Song X, Lei L, et al. 3D printing of piezoelectric element for energy focusing and ultrasonic sensing. Nano Energy 2016, **27**: 78-86.

[14] Zeng Y, Jiang L, Sun Y, et al. 3D-Printing Piezoelectric Composite with Honeycomb Structure for Ultrasonic Devices. Micromachines 2020, **11**: 713.

[15] Cheng J, Chen Y, Wu JW, et al. 3D Printing of $BaTiO_3$ Piezoelectric Ceramics for a Focused

Ultrasonic Array. Sensors 2019, **19**: 4078.

[16] Chen Z, Sun X, Shang Y, et al. Dense ceramics with complex shape fabricated by 3D printing: A review. Journal of Advanced Ceramics 2021, **10**: 195-218.

[17] Liu Y, Lian H, Chen X. Effect of particle size of precursor powders on structure and electrical properties of $(Pb_{0.945}Bi_{0.027}La_{0.01})(Nb_{0.95}Ti_{0.0625})_2O_6$ piezoelectric ceramics. Journal of Shaanxi Normal University 2016, **44**: 49-56.

[18] Yu H, Wang X, Jian F, et al. Grain Size Effects on Piezoelectric Properties and Domain Structure of BaTiO3 Ceramics Prepared by Two-Step Sintering. Journal of the American Ceramic Society 2013, **96**: 3369-3371.

[19] Griffith ML, Halloran JW. Scattering of ultraviolet radiation in turbid suspensions. Journal of Applied Physics 1997, **81**: 2538-2546.

[20] Kaully T, Siegmann A, Shacham D. Rheology of highly filled natural $CaCO_3$ composites. II. Effects of solid loading and particle size distribution on rotational rheometry. Polymer Composites 2010, **28**: 524-533.

[21] Sun C, Zhang X. The influences of the material properties on ceramic micro-stereolithography. Sensors & Actuators A Physical 2016, **101**: 364-370.

[22] Yoon B K, Lee B A, Kang S. Growth behavior of rounded (Ti,W)C and faceted WC grains in a Co matrix during liquid phase sintering. Acta Materialia 2005, **53**: 4677-4685.

[23] Renteria A, Diaz JA, He B, et al. Particle size influence on material properties of $BaTiO_3$ ceramics fabricated using freeze-form extrusion 3D printing. Materials Research Express 2019, **6**: 115211.

[24] Yan W, Yu S, Deng X, et al. Dielectric and Ferroelectric Properties of $BaTiO_3$ Nanofibers Prepared via Electrospinning. Journal of Materials Science & Technology 2014, **30**: 743-747.

[25] Tan Y, Zhang J, Wu Y, et al. Unfolding grain size effects in barium titanate ferroelectric ceramics. Scientific Reports 2015, **5**: 9953.

[26] Huang YA, Biao LU, Zou YX, et al. Grain Size Effect on Dielectric, Piezoelectric and Ferroelectric Property of $BaTiO_3$ Ceramics with Fine Grains. Journal of Inorganic Materials 2018, **33**: 767-772.